MAGNETOHYDRODYNAMICS Vol. 57 (2021), No. 3, pp. 337–351
DOI: 10.22364/mhd.57.3.4

SORET–DUFOUR IMPACTS ON INCLINED MAGNETIC CASSON FLUID FLOW

S. Parvin [1], *S.S.P.M. Isa* [1,2,*], *N.M. Arifin* [1,3], *F.M. Ali* [1,3]

[1] *Institute for Mathematical Research, University Putra Malaysia, 43400 UPM Serdang, Selangor Darul Ehsan, Malaysia*
[2] *Centre of Foundation Studies for Agricultural Science, University Putra Malaysia, 43400 UPM Serdang, Selangor Darul Ehsan, Malaysia*
[3] *Department of Mathematics, University Putra Malaysia, 43400 UPM Serdang, Selangor Darul Ehsan, Malaysia*
[*] *Corresponding author's email: ctsuzilliana@upm.edu.my*

In industrial processes such as the paper production, reservoir engineering and thermal retrieval process, combined Soret and Dufour effects are involved. Also, the Soret–Dufour effect has been used in the chemical industry for detachment, purification, and radioactive nuclear waste material. Therefore, a mathematical model of Soret–Dufour effects in a Casson fluid flow caused by a shrinking sheet is presented in this paper. This model is subjected to an inclined magnetic field, along with the exponential variations of the variables at the sheet, i.e. velocity, temperature, and concentration. Ordinary differential equations for momentum, energy, and concentration are solved numerically using the `bvp4c` MATLAB program. At the end of the calculations, the profiles of velocity, temperature and concentration are displayed. In addition, the skin friction coefficient, the local Nusselt number and the local Sherwood number are also considered. Numerical results of velocity, temperature, and concentration profiles, together with the skin friction coefficient, local Nusselt number and local Sherwood number are shown in the form of tables and graphs. The numerical results show that the skin friction coefficient and the local Sherwood number decrease, whereas the temperature profile and the local Nusselt number for the first solution increase with the increment of the Soret number. Velocity and concentration profiles decrease with the increment of the Dufour number.

Introduction.

The combined heat and mass transfer in a fluid flow contributes to compressed heat exchangers, heat insulation, drying technology, paper processing, and catalytic reactors [1]. When the temperature gradient arises, a mass in the fluid will be transferred. On the one hand, heat is transferred in a fluid medium when there is a concentration gradient. These mass and heat transfers are recognized as Soret and Dufour effects, respectively. Therefore, researchers are encouraged to consider the Soret–Dufour impact in their fluid flow model if combined heat and mass transfer effects coincide. Moreover, experimental works have reported that the temperature and concentration gradients must be enormous to make the Soret–Dufour parameters effectively show their impacts [2]. On the other hand, the fluid flow in the stretching or shrinking sheet system have found industrial application in the following processes: glass fiber and paper production, extrusion of polymer sheet from a die and continuous casting [3]. Therefore, the impacts of the Soret–Dufour parameters in a mathematical model of fluid flow, as stated in the industrial applications above, are reported [1, 2, 4–14]. The velocity function of the sheet is assumed to be linear, non-linear, or exponential.

Previous studies have established a linear function due to the Soret-Dufour effects at the early stage of research [1, 4–7]. Bhattacharya *et al.* [1] solved a mathematical model of fluid flow near a stagnation point. The Soret-Dufour effect in a three-dimensional model of nanofluid was described by Ramzan *et al.* [4]. Soret and Dufour effects on the

Oldroyd-B fluid flow in a model of two and three-dimensional Cartesian coordinates were studied by Ashraf *et al.* [5] and Farooq *et al.* [6], respectively. Peristaltic motion with Soret and Dufour effects was investigated by Hayat *et al.* [7].

Subsequently, a mathematical model of Soret–Dufour effects due to a non-linear stretching/shrinking sheet has been developed [2, 8, 9]. Pal and Mondal [2] studied a mixed convection radiating fluid flow and heat and mass transfer in a non-Darcian porous medium. The effect of thermal radiation and convective boundary condition in nanofluids was investigated by Pal *et al.* [8]. The unsteady state of Casson fluid flow bounded by slipped and convected boundary conditions was analyzed by Ullah *et al.* [9].

Meanwhile, some researchers combined the exponential variations of the sheet velocity with the Soret–Dufour effects [10–14]. For example, Srinivasacharya and RamReddy [10] made numerical solutions of a Newtonian fluid flow. Subsequently, their studies [10] were expanded by Sreenivasulu and Reddy [11] by calculating other impacts, such as thermal radiation and viscous dissipation. However, the results published by Srinivasacharya and RamReddy [10] and by Sreenivasulu and Reddy [11] were restricted to a two-dimensional mathematical model. Therefore, a three-dimensional mathematical model of Newtonian fluid affected by the Soret–Dufour parameters was reported by Hayat *et al.* [12]. Moreover, their model was subjected to chemical reactions and heat source/sink. On the other hand, Sharada and Shankar [13] used the Casson fluid mathematical formulation and added it to the governing equations derived by Srinivasacharya and RamReddy [10]. In addition, Sharada and Shankar [13] added the effects of thermal radiation and chemical reactions to their model problem. Recently, Isa *et al.* [14] extended the model of Srinivasacharya and Reddy [10] by using a different range of controlling parameters.

Nevertheless, Soret-Dufour impacts on convection, where the medium that acts as a boundary of the fluid has a specific condition/state/shape, were reported recently for different types of fluids. For example, the exponential function of the inclined stretching sheet in magnetohydrodynamic (MHD) Newtonian and Casson fluids was investigated by Sravanthi [15] and Chandra Sekhar and Manjula [16], respectively. MHD mixed convection over an inclined flat plate with the effects of Soret-Dufour numbers, non-uniform heat source/sink and chemical reaction was studied by Mondal *et al.* [17]. The presence of thermal radiation and viscous dissipation in the system of steady axisymmetric flow beyond an inclined stretching cylinder was studies by Hayat *et al.* [18]. A three-dimensional MHD mixed convection flow past an infinite vertical porous plate with thermal radiation has been analyzed by Ahmed and Sengupta [19]. Jamsed and Kottakkaran [20] worked with a Williamson nanofluid in a parabolic trough solar collector. Jamshed *et al.* extended their work with Casson nanofluids, namely, copper–ethylene glycol and molybdenum disulfide–ethylene glycol [21] and Ag-Cu/EO Williamson hybrid nanofluid [22]. As a continuation of the above work [20], Jamshed *et al.* [23] focused on the effect of radiative heat transfer in a second-grade nanofluid (copper engine oil and alumina engine oil) flow. Hayat *et al.* [24] studied an MHD Newtonian fluid flow bounded by an exponentially curved surface.

In the mathematical model of fluid flow, there is a high possibility to obtain multiple solutions. Firstly, a reliable solution in an actual fluid situation must be chosen. For that reason, a comparison with the experimental results can be made. This can be done by implementing calculations known as stability analysis. This analysis determines two types of solutions: stable or unstable. It is developed through `bvp4c` program from MATLAB. The application of stability analysis in the related cases has been made by some researchers [14, 25–27]. A copper-water nanofluid flow over a slipped boundary

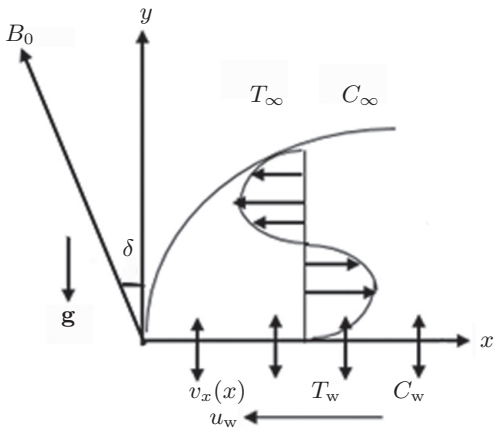

Fig. 1. Schematic diagram of the model problem.

was examined by Dzulkifli *et al.* [25]. Subsequently, Dzulkifli *et al.* [26] extended their works from [25] for the unsteady state. Recently, a stability analysis was performed by Najib *et al.* [27] to revise the case of a nanofluid stagnation point flow past a shrinking/stretching sheet, including second-order slip at boundary conditions.

The studies of MHD Casson fluid over an exponentially flat shrinking sheet have been performed by Parvin *et al.* [28, 29], where the stability analysis was also included [29]. However, these studies are restricted to the case when the vector of the transverse magnetic field is located at the vertical axis of the fluid flow system. Therefore, this paper extends the studies when the magnetic field is projected at a certain angle from the vertical direction with the Soret–Dufour effects.

1. Methodology.

Let us consider a two-dimensional model of an incompressible, viscous and electrically conducting fluid [28, 29] with an extended version (inclined magnetic field vector). The main vectors arising in this system are a shrinking sheet (at the x-axis) and an inclined magnetic field (projected from the y-axis by an inclination angle [30]). The model for the recent problem is presented in Fig. 1.

1.1. Continuity equation.

The continuity equation is stated as

$$\frac{\partial u}{\partial x} + \frac{\partial v}{\partial y} = 0. \tag{1}$$

Here u and v are the components of velocity in the x- and y-directions with $u = \partial\psi/\partial y$ and $v = -\partial\psi\partial y$. The stream function is

$$\psi(x, y) = \sqrt{2\upsilon L U_0}\, \mathrm{e}^{x/2L} f(\eta). \tag{2}$$

The boundary layer thickness is defined as

$$\eta = \sqrt{\frac{U_0}{2\upsilon L}}\, y \mathrm{e}^{x/2L}.$$

Then, u and v are transformed into

$$u = U_0 f'(\eta)\,\mathrm{e}^{x/L}, \quad v = -\sqrt{\frac{\upsilon U_0}{2L}}\,\mathrm{e}^{x/2L}[f(\eta) + (\eta)f'(\eta)], \tag{3}$$

where prime denotes the differentiation with respect to η. Since u and v satisfy the continuity equation, we can proceed to the following governing equations.

1.2. Momentum equation.

The second governing equation is known as the momentum equation:

$$u\frac{\partial u}{\partial x} + v\frac{\partial u}{\partial y} = \nu\left(1 + \frac{1}{\omega}\right)\frac{\partial^2 u}{\partial y^2} + \beta_{\mathrm{T}}(T - T_\infty)g + \beta_{\mathrm{C}}(C - C_\infty)g - \frac{\sigma B_0^2 u}{\rho}\sin^2(\delta), \tag{4}$$

where $\nu = \mu/\rho$ is the kinematic viscosity, μ is the viscosity, ρ is the fluid density, ω is the Casson parameter, g is the acceleration due to gravity, β_{T} is the thermal expansion coefficient, β_{C} is the solutal expansion coefficient, δ is the inclined angle of the magnetic field, σ is the electrical conductivity, B_0 is the constant strength of the magnetic field, the fluid temperature is T and the fluid concentration is C. The subscripts 'w' and '∞' at the parameters T and C indicate the conditions at the wall and at the outer edge of the boundary layer, respectively. The formulation of the Casson fluid ω in Eq. (4) has been derived in [31]. Introducing two new similarity variables yields

$$\theta(\eta) = (T - T_\infty)/(T_{\mathrm{w}} - T_\infty), \quad \varphi(\eta) = (C - C_\infty)/(C_{\mathrm{w}} - C_\infty). \tag{5}$$

By using Eq. (3) and Eq. (5), Eq. (4) is transformed as

$$\left(\frac{\omega + 1}{\omega}\right) f''' + f''f - 2(f')^2 - 2\mathrm{H}\sin^2(\delta)f' + 2\mathrm{Ri} \times (\theta + \mathrm{N}\varphi) = 0, \tag{6}$$

where

$$\mathrm{Ri} = 2\frac{gB_{\mathrm{T}}T_0 L}{U_0^2}\,\mathrm{e}^{-3x/2L}$$

is a mixed convection parameter,

$$\mathrm{H} = \frac{\sigma L B_0^2}{\rho U_0}\,\mathrm{e}^{-x/L}$$

is a magnetic field parameter and

$$\mathrm{N} = \frac{\beta_{\mathrm{C}}}{\beta_{\mathrm{T}}}\frac{C_{\mathrm{w}} - C_\infty}{T_{\mathrm{w}} - T_\infty}$$

is a buoyancy ratio parameter. Hence, a stability analysis is performed and the dimensionless time variable τ is introduced [32]. The new governing momentum equation is

$$\frac{\partial u}{\partial t} + u\frac{\partial u}{\partial x} + v\frac{\partial u}{\partial y} = \left(\frac{\omega + 1}{\omega}\right)\upsilon\frac{\partial^2 u}{\partial y^2} + \beta_{\mathrm{T}}(T - T_\infty)g + \beta_{\mathrm{C}}(C - C_\infty)g - \frac{\sigma B_0^2 u}{\rho}\sin^2(\delta), \tag{7}$$

and the similarity variables are

$$\begin{gathered}\theta(\eta,\tau) = \frac{T - T_\infty}{T_{\mathrm{w}} - T_\infty}, \quad \varphi(\eta,\tau) = \frac{C - C_\infty}{C_{\mathrm{w}} - C_\infty}, \\ \tau = \frac{U_0 t}{2L}\,\mathrm{e}^{x/L}, \quad \eta = y\sqrt{\frac{U_0}{2\upsilon L}}\,\mathrm{e}^{x/2L}.\end{gathered} \tag{8}$$

Substituting equation Eq. (8) into Eq. (7) yields

$$\left(1+\frac{1}{\omega}\right)\frac{\partial^3 f}{\partial\eta^3}+f\frac{\partial^2 f}{\partial\eta^2}-2\left(\frac{\partial f}{\partial\eta}\right)^2+2\mathrm{Ri}\theta+2\mathrm{RiN}\varphi-\\ \frac{\partial^2 f}{\partial\eta\partial\tau}+2\tau\frac{\partial f}{\partial\tau}\frac{\partial^2 f}{\partial\eta^2}-2\tau\frac{\partial f}{\partial\eta}\frac{\partial^2 f}{\partial\eta\partial\tau}-2\mathrm{H}\sin^2(\delta)\frac{\partial f}{\partial\eta}=0. \tag{9}$$

The analysis introduced by previous studies in stability field [32] is as below

$$\begin{aligned} f(\eta,\tau)-f_0(\eta)&=\mathrm{e}^{-\gamma\tau}P(\eta,\tau),\\ \theta(\eta,\tau)-\theta_0(\eta)&=\mathrm{e}^{-\gamma\tau}Q(\eta,\tau),\\ \varphi(\eta,\tau)-\varphi_0(\eta)&=\mathrm{e}^{-\gamma\tau}R(\eta,\tau), \end{aligned} \tag{10}$$

where γ represents an eigenvalue, whereas $P(\eta,\tau)$, $Q(\eta,\tau)$ and $R(\eta,\tau)$ are small compare to $f_0(\eta)$, $\theta_0(\eta)$ and $\varphi_0(\eta)$. Next, by using Eq. (10) into Eq. (9) and inserting $\tau=0$, the following equation is derived

$$\left(1+\frac{1}{\omega}\right)P_0'''+f_0P_0''+f_0''P_0-f_0'P_0'+2\mathrm{Ri}(Q_0+\mathrm{N}R_0)+[\gamma-2\mathrm{H}\sin^2(\delta)]P_0'=0. \tag{11}$$

1.3. Energy equation.

The third governing equation reads as

$$u\frac{\partial T}{\partial x}+v\frac{\partial T}{\partial y}=\alpha\frac{\partial^2 T}{\partial y^2}+\frac{(DK_\mathrm{T})}{(C_\mathrm{P}C_\mathrm{S})}\frac{\partial^2 C}{\partial y^2}, \tag{12}$$

where the thermal diffusivity is α, the thermal diffusion ratio is K_T, the medium solutal diffusivity is D, the concentration susceptibility is C_S and the specific heat at constant pressure is C_P. When Eq. (3) and Eq. (5) are substituted into Eq. (12) the following equation is derived

$$\frac{1}{\mathrm{Pr}}\theta''+\mathrm{Du}\varphi''-f'\theta+f\theta'=0. \tag{13}$$

Here $\mathrm{Pr}=\upsilon/\alpha$ is the Prandtl number and $\mathrm{Du}=[DK_\mathrm{T}(C_\mathrm{w}-C_\infty)]/[C_\mathrm{S}C_\mathrm{P}\upsilon(T_\mathrm{w}-T_\infty)$ is the Dufour number. Next, a new governing energy equation is introduced to perform the stability analysis.

$$\frac{\partial T}{\partial t}+u\frac{\partial T}{\partial x}+v\frac{\partial T}{\partial y}=\alpha\frac{\partial^2 T}{\partial y^2}+\frac{(DK_\mathrm{T})}{(C_\mathrm{P}C_\mathrm{S})}\frac{\partial^2 C}{\partial y^2}. \tag{14}$$

Substituting Eq. (8) into Eq. (14) yields

$$\frac{1}{\mathrm{Pr}}\frac{\partial^2\theta}{\partial\eta^2}+\mathrm{Du}\frac{\partial^2\varphi}{\partial\eta^2}+f\frac{\partial\theta}{\partial\eta}-\theta\frac{\partial f}{\partial\eta}-\frac{\partial\theta}{\partial\tau}-2\tau\frac{\partial f}{\partial\eta}\frac{\partial\theta}{\partial\tau}+2\tau\frac{\partial f}{\partial\tau}\frac{\partial\theta}{\partial\eta}=0. \tag{15}$$

And using Eq. (10) in Eq. (15), the following equation is derived

$$\frac{1}{\mathrm{Pr}}Q_0''+\mathrm{Du}R_0''+f_0Q_0'-Q_0f_0'+\theta_0'P_0-\theta_0P_0'+\gamma Q_0=0. \tag{16}$$

1.4. Concentration equation.

The last governing equation is known as the concentration equation:

$$u\frac{\partial C}{\partial x}+v\frac{\partial C}{\partial y}=D\left[\frac{\partial^2 C}{\partial y^2}+\frac{K_{\mathrm{T}}}{T_{\mathrm{m}}}\frac{\partial^2 T}{\partial y^2}\right], \tag{17}$$

where T_{m} is known as the mean fluid temperature. Using similarity transformation, Eqs. (3) and (5) substituted into Eq. (17) yield the following equation:

$$\frac{1}{\mathrm{Sc}}\varphi''+\mathrm{Sr}\,\theta''-f'\varphi+f\varphi'=0, \tag{18}$$

where $\mathrm{Sc}=\upsilon/D$ is the Schmidt number and $\mathrm{Sr}=[DK_{\mathrm{T}}(T_{\mathrm{w}}-T_{\infty})]/[T_m\upsilon(C_{\mathrm{w}}-C_{\infty})]$ is the Soret number. For the stability analysis, the concentration equation is taken as

$$\frac{\partial C}{\partial t}+u\frac{\partial C}{\partial x}+v\frac{\partial C}{\partial y}=D\left[\frac{\partial^2 C}{\partial y^2}+\frac{K_{\mathrm{T}}}{T_{\mathrm{m}}}\frac{\partial^2 T}{\partial y^2}\right]. \tag{19}$$

Substituting Eq. (8) into Eq. (19) yields

$$\frac{1}{\mathrm{Sc}}\frac{\partial^2\varphi}{\partial\eta^2}+\mathrm{Sr}\frac{\partial^2\theta}{\partial\eta^2}+f\frac{\partial\varphi}{\partial\eta}-\varphi\frac{\partial f}{\partial\eta}-\frac{\partial\varphi}{\partial\tau}-2\tau\frac{\partial f}{\partial\eta}\frac{\partial\varphi}{\partial\tau}+2\tau\frac{\partial f}{\partial\tau}\frac{\partial\varphi}{\partial\eta}=0, \tag{20}$$

and using Eq. (10) in Eq. (20) we derive

$$\frac{1}{\mathrm{Sc}}R_0''+\mathrm{Sr}\,Q_0''+f_0R_0'-R_0f_0'+\varphi_0'F_0-\varphi_0F_0'+\gamma R_0=0. \tag{21}$$

1.5. Boundary conditions.

The mathematical formulation in this paper is determined by the following boundary conditions:

$$\begin{gathered}u_{\mathrm{w}}(x)=u=\lambda U_0\mathrm{e}^{x/L},\quad v_{\mathrm{w}}(x)=v=-S\sqrt{\frac{\upsilon U_0}{2L}}\mathrm{e}^{x/2L},\\ T_{\mathrm{w}}(x)=T_{\infty}+T_0\mathrm{e}^{x/2L},\quad C_{\mathrm{w}}(x)=C_{\infty}+C_0\mathrm{e}^{x/2L},\quad \text{at } y=0,\\ u\to 0,\quad T\to T_{\infty},\quad C\to C_{\infty},\quad \text{as } y\to\infty,\end{gathered} \tag{22}$$

where the negative λ denotes the shrinking parameter, $v_{\mathrm{w}}(x)$ is the mass transfer velocity and $S>0$ is the suction parameter. Using the similarity transformation Eq. (3) and Eq. (5) we obtain

$$\begin{gathered}f'(0)=\lambda,\quad f(0)=\lambda,\quad \theta(0)=1,\quad \phi(0)=1,\quad \text{at } \eta=0,\\ f'(\infty)\to 0,\quad \theta(\infty)\to 0,\quad \phi(\infty)\to 0,\quad \text{as } \eta\to\infty.\end{gathered} \tag{23}$$

The boundary conditions for the stability analysis are

$$\begin{gathered}\frac{\partial f}{\partial\eta}(0,\tau)=\lambda,\quad f(0,\tau)=S,\quad \theta(0,\tau)=1,\quad \varphi(0,\tau)=1\quad \text{at } \eta=0,\\ \frac{\partial f}{\partial\eta}(\infty,\tau)\to 0,\quad \theta(\infty,\tau)\to 0,\quad \varphi(\infty,\tau)\to 0\quad \text{as } \eta\to\infty.\end{gathered} \tag{24}$$

Next, applying Eq. (10) in Eq. (24) yields

$$\begin{aligned} &P_0'(0)=0, \quad P_0(0)=0, \quad Q_0(0)=0, \quad R_0(0)=0, \quad \text{at } \eta=0,\\ &P_0'(\infty)\to 0, \quad Q_0(\infty)\to 0, \quad R_0(\infty)\to 0, \quad \text{as } \eta\to\infty. \end{aligned} \tag{25}$$

For the considered problem, the first boundary condition as $\eta\to\infty$ is relaxed. The relaxation technique of boundary conditions has been described in [33]. A numerical computation in the MATLAB `bvp4c` programme is performed by using Eqs. (6), (13), (18) and (22). Subsequently, Eqs. (11), (16) and (21), including the new boundary conditions $P_0''(0)=1$, are used in the MATLAB `bvp4c` programme for stability analysis. The physical parameters C_f (skin friction coefficient), Nu_x (local Nusselt number) and Sh_x (local Sherwood number) are presented as

$$C_\mathrm{f}=\frac{\mu}{\rho U_0^2}\frac{\partial u}{\partial y}, \ \mathrm{Nu}_x=-\frac{L}{T_\mathrm{w}-T_\infty}\left(\frac{\partial T}{\partial y}\right)_{y=0}, \ \mathrm{Sh}_x=-\frac{L}{C_\mathrm{w}-C_\mathrm{m}}\left(\frac{\partial C}{\partial y}\right)_{y=0}. \tag{26}$$

Substituting Eq. (3) and Eq. (5) into Eq. (26) then yields

$$\sqrt{2\mathrm{Re}_x}\mathrm{e}^{-3x/2}C_\mathrm{f}=f''(0), \ \mathrm{Nu}_x\sqrt{\frac{2}{\mathrm{Re}_x}}\mathrm{e}^{-x/2}=-\theta'(0), \ \mathrm{Sh}_x\sqrt{\frac{2}{\mathrm{Re}_x}}\mathrm{e}^{-x/2}=-\varphi'(0), \tag{27}$$

where $\mathrm{Re}_x=(U_0L)/\nu\mathrm{e}^{x/L}$ is the Reynolds number.

2. Results and discussion.

In the present study, the subsequent values are considered for the whole MatLab program unless otherwise stated: $\lambda=-0.4$, $\omega=2000$, $\mathrm{S}=2.5$, $\mathrm{N}=1.0585$, $\delta=80°$, $\mathrm{Sc}=0.5$, $\mathrm{Ri}=-0.0212$, $\mathrm{H}=0.4946$, $\mathrm{Pr}=1$, $\mathrm{Sr}=1.8004$, $\mathrm{Du}=0.1002$. For the numerical values of the wall temperature gradient $\theta'(0)$, a comparison with previous results [34] is made for different values of the Prandtl number Pr, as shown in Table 1. As a result, those values are found to be in good agreement with the previous findings [10, 34].

In Figs. 2–5, the first and second solutions are indicated by a solid and a dashed line, respectively. The first solution is considered stable, whereas the other one is unstable. The stability analysis provides positive eigenvalues for the first solution. Otherwise, their values are negative. In addition, the stable solution always follows the conditions at the boundary, Eq. (23), with minimum existence of minimum or maximum peaks. These

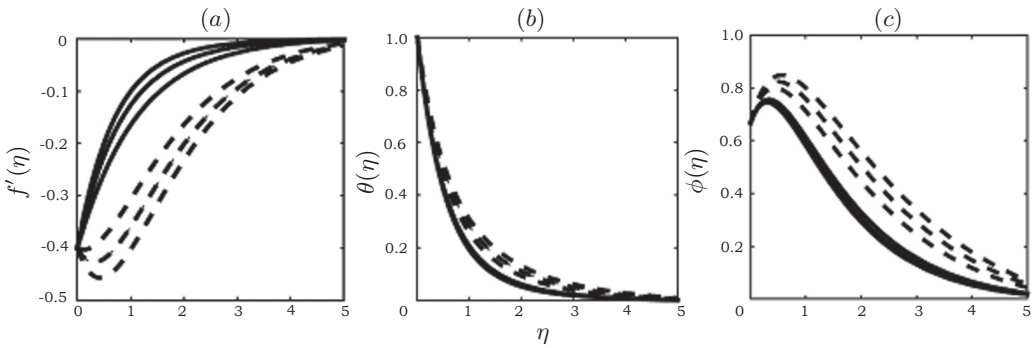

Fig. 2. The first and second solutions on the profiles of (*a*) velocity, (*b*) temperature, and (*c*) concentration.

Table 1. Comparison of wall temperature gradients $\theta'(0)$ for $S = H = Ri = Sc = Sr = Du = N = \delta = 0$ and $\omega = 1000000$.

λ	Pr	[34]	[10]	Present
1	0.5	-0.59434	-0.59438	-0.59466
	1.0	-0.95478	-0.95478	-0.95478
	3.0	-1.86908	-1.86908	-1.86907
0.86470	0.5	—	—	-0.55322
	1.0			-0.88785
	3.0			-1.73804

Table 2. The smallest eigenvalues when $S = 1.685$ for dual solutions.

		Solutions	
Du	Sr	First Solution	Second Solution
0.1	1.8000	0.08257	-0.08545
	1.8002	0.08253	-0.08541
	1.8004	0.08248	-0.08536
0.1002	1.8000	0.08247	-0.08534
	1.8002	0.08242	-0.08529
	1.8004	0.08238	-0.08525

stable and unstable solutions in Fig. 2 are plotted for $\eta \leq 5$. The numerical values of the stability analysis are listed in Table 2 which reports the smallest eigenvalues γ. Table 1 shows the positive eigenvalues for the first solution, and negative for the other solution.

Fig. 3 illustrates the impact of the Soret number Sr and Dufour number Du on velocity profiles. In Fig. 3*a*, it is observed that, due to the augmentation of the Soret number, the velocity profile of the first solution decreases for the whole range of the momentum boundary layer thickness. The magnitude of the instantaneous velocity of the first solution decreases until the velocity becomes zero. Hence, the zero velocity indicates no fluid movement. Besides, the Sr effect causes a decrement in the second solution close to the shrinking sheet. The velocity profiles for the second solution decrease at a small η and reach a minimum point, and then it increases until it achieves the zero value. The velocity profiles for different values of Du are shown in Fig. 3*b*. It is observed that with increasing Du the velocity of the first and second solutions is found to decrease. This decrease can be seen for the whole range of η for the first solution and at large η for the second solution. However, the effect of Du is to increase the velocity profile for the second solution and at the small η.

Fig. 4 and Fig. 5 show the impact of Sr and Du on the temperature $\theta(\eta)$ and concentration $\varphi(\eta)$ profiles, respectively. Fig. 4 shows the continuous decrement of instantaneous temperature for different fluid thickness η for both Sr and Du. It is found that the temperature distribution increases with increasing Sr and Du for both solutions. From Fig. 4*a* it is clear that the concentration profiles increase due to the addition of Sr for both solutions. On the other hand, the effect of Du should decrease the concentration profile at small η (close to the shrinking sheet), but the concentration level is enhanced due to the impact of the same parameter at large η (far from the sheet) for both solutions (Fig. 5*b*).

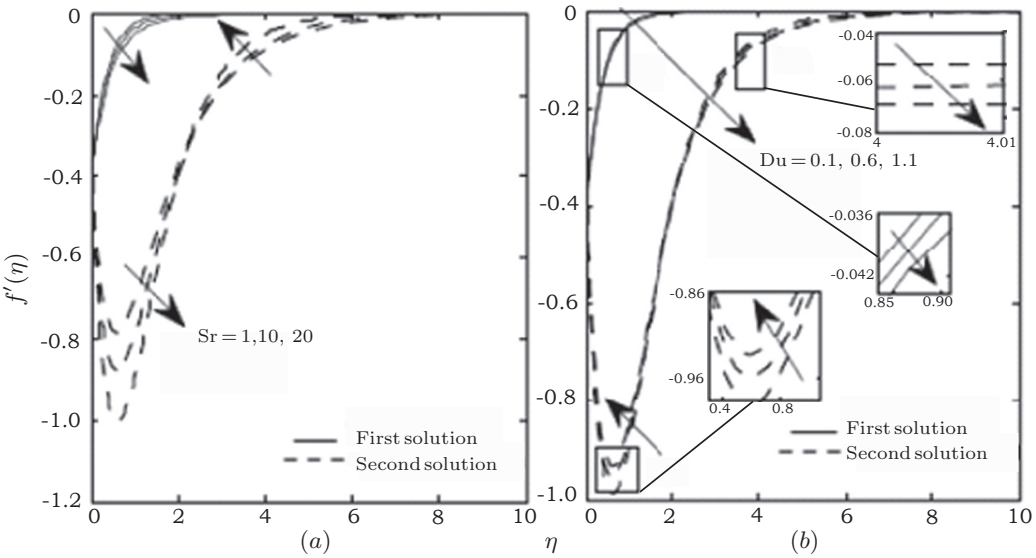

Fig. 3. Impact of (*a*) the Soret number Sr and (*b*) Dufour number Du on the velocity profile.

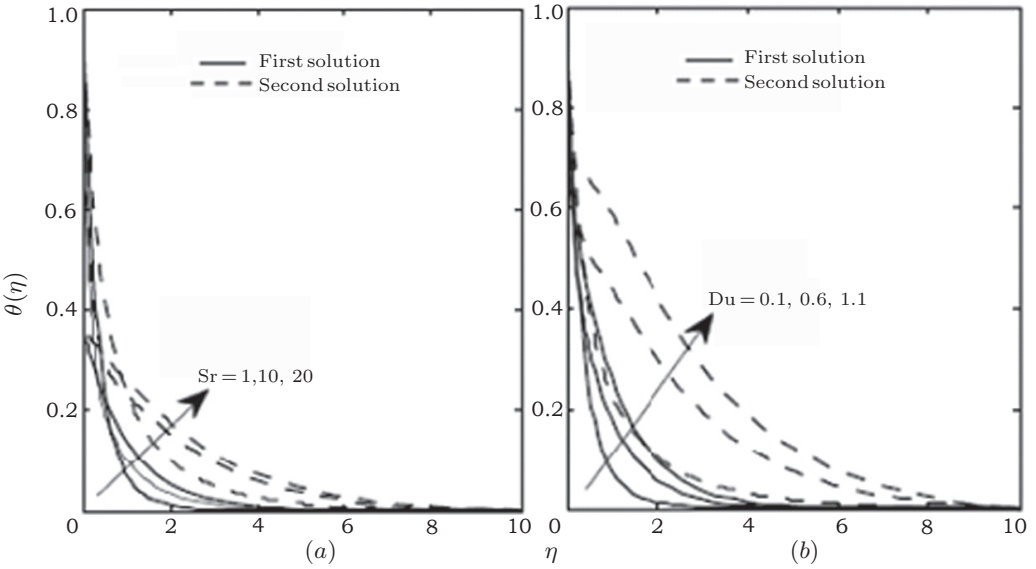

Fig. 4. Impact of (*a*) the Soret number Sr and (*b*) Dufour number Du on the temperature profile.

From Figs. 3–5, it can be seen that Sr and Du have opposite characteristics. These characteristics are described in the first solution only because this solution is stable and physically reliable. The Soret effect recognizes the mass transfer from the lower to the higher concentration due to the temperature gradient. Therefore, the concentration increases due to the increment of the Soret number (Fig. 5*a*). In other words, Du has the opposite impact on $\varphi(\eta)$, where it decreases the value of $\varphi(\eta)$ (Fig. 5*b*) at a distance close to the shrinking sheet. The concentration gradient induces heat transfer from the lower to the higher temperature profile, which is labelled as the Dufour effect. As a result, Fig. 4*b* shows that large Du increases the temperature and the thickness of the thermal layer.

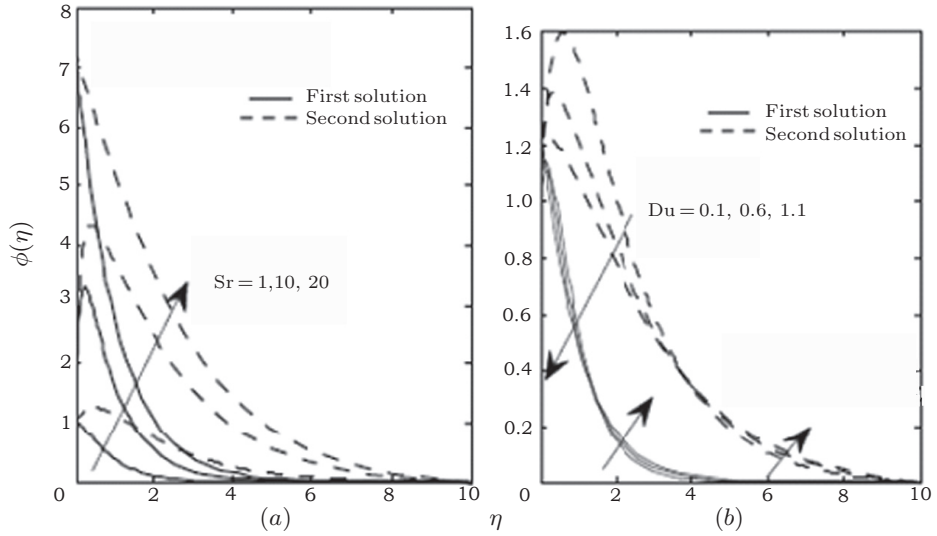

Fig. 5. Impact of (*a*) the Soret number Sr and (*b*) Dufour number Du on the concentration profile.

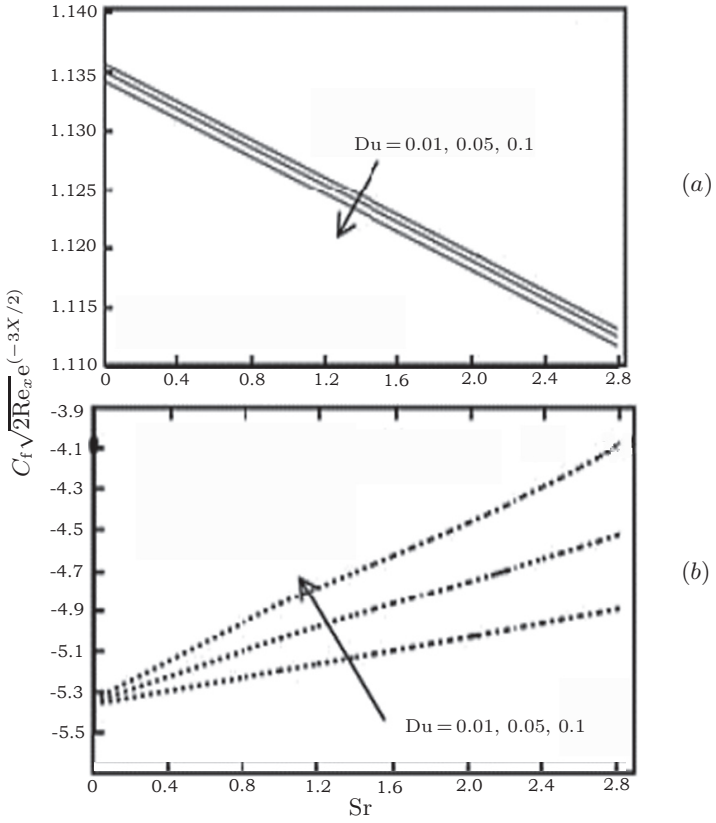

Fig. 6. Graphical presentation of the skin friction coefficient $C_f\sqrt{2\mathrm{Re}_x}e^{(-3X/2)}$ vs. the Soret number for different values of the Dufour number: (*a*) first solution, (*b*) second solution.

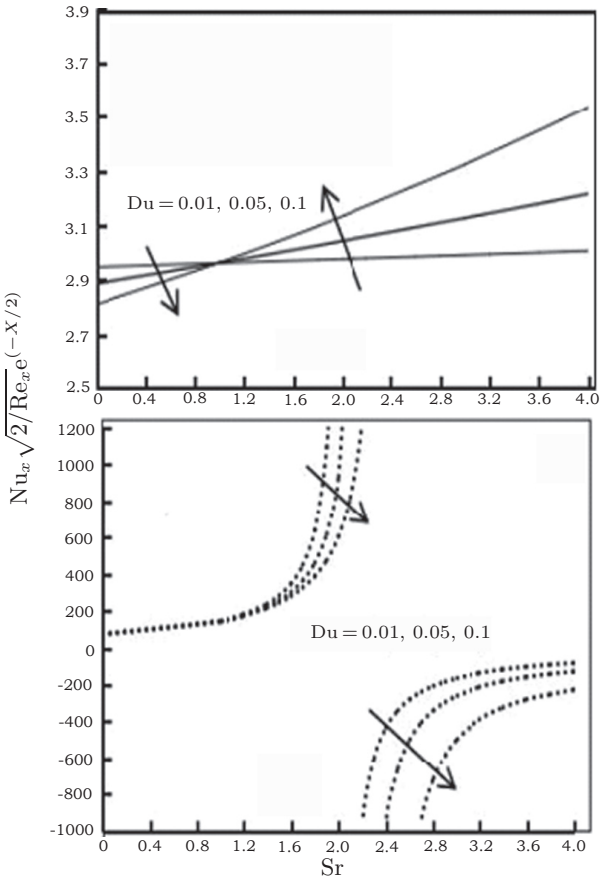

Fig. 7. Graphical presentation of the local Nusselt number $\mathrm{Nu}_x\sqrt{2/\mathrm{Re}_x}\mathrm{e}^{(-X/2)}$ vs. the Soret number for different values of the Dufour number: (*a*) first solution, (*b*) second solution.

In Figs. 6–8, the first and second solutions are indicated by a solid and a dotted line, respectively. The distribution of the skin friction coefficient $C_\mathrm{f}\sqrt{2\mathrm{Re}_x}\mathrm{e}^{-3x/2}$ is displayed in Fig. 6. From this figure, it is seen that the skin friction coefficient declines with the inclination of Sr and Du for the first solution and it seems parallel in the whole range of Sr. However, with the increase of Sr and Du for the second solution, the skin friction coefficient increases. The variation of the local Nusselt number $\sqrt{(2/\mathrm{Re}_x)}\mathrm{Nu}_x\mathrm{e}^{-x/2}$ is presented in Fig. 7. This figure demonstrates that the local Nusselt number of the first solution decreases when the Dufour parameter increases, with a small value of the Soret parameter. However, an opposite pattern is observed for the local Nusselt number, with a larger Sr. For the second solution, the local Nusselt number versus the Soret number shows the presence of positive $\mathrm{Nu}_x\sqrt{(2/\mathrm{Re}_x)}\mathrm{e}^{-x/2}$ for small Sr and negative $\mathrm{Nu}_x\sqrt{(2/\mathrm{Re}_x)}\mathrm{e}^{-x/2}$ for large Sr. In addition, Fig. 7 shows that the values of $\mathrm{Nu}_x\sqrt{(2/\mathrm{Re}_x)}\mathrm{e}^{(-x/2)}$ decrease with increasing Du. The local Sherwood number $\sqrt{(2/\mathrm{Re}_x)}\mathrm{Sh}_x\mathrm{e}^{(-x/2)}$ is displayed in Fig. 8. It is seen that the local Sherwood number declines with the inclination of Sr and Du for the first solution. However, for small Sr, this change is negligible. For the second solution, the negative and positive regions of the local Sherwood number $\sqrt{(2/\mathrm{Re}_x)}\mathrm{Sh}_x\mathrm{e}^{-x/2}$ occur at the small and the large Soret

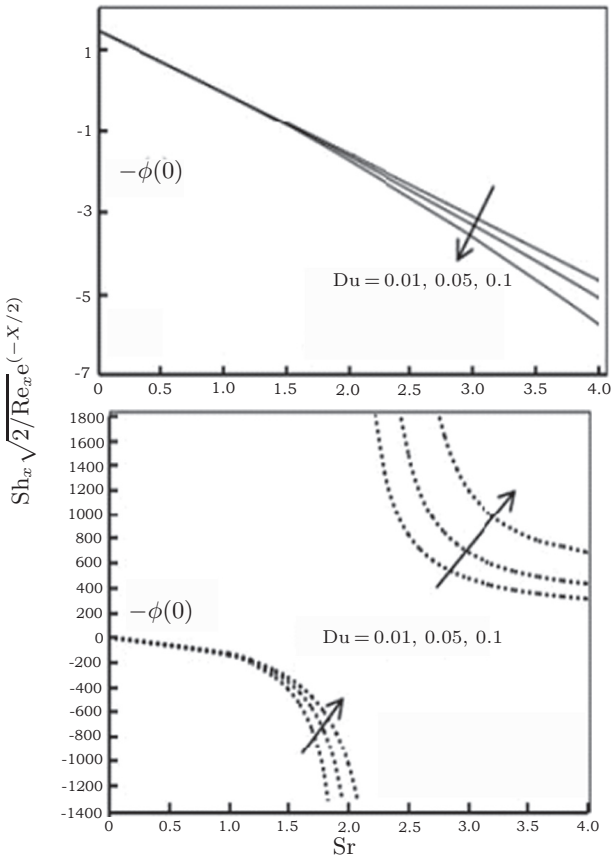

Fig. 8. Graphical presentation of the local Sherwood number $\mathrm{Sh}_x\sqrt{2/\mathrm{Re}_x}\mathrm{e}^{(-X/2)}$ vs. the Soret number Sr for different values of the Dufour number Du: (a) first solution, (b) second solution.

number, respectively. Fig. 8 also displays the increment of the local Sherwood number $\mathrm{Sh}_x\sqrt{(2/\mathrm{Re}_x)}\mathrm{e}^{-x/2}$ with the increase of Du.

Conclusions.

From the results presented as tables and graphs, the main conclusions are as follows.

- The Soret number contributes to the increment of the temperature profile for both solutions, and the local Nusselt number contributes to the first solution.
- The impact of the Dufour number is to decrease the rate of velocity and concentration of the Casson fluid for both solutions. This decrease can be observed for the large momentum boundary layer thickness and for the small thickness of the concentration boundary layer.
- An increase in Soret number causes a decrease of the skin friction coefficient and local Sherwood number for the first solution. In contrast, the same parameter increases the local Nusselt number in the first solution.
- The effect of the Dufour number causes the increasing function of the skin friction coefficient of the second solution, of the local Nusselt number of the first solution at

the enormous value of the Soret number, and of the local Sherwood number of the second solution.

Acknowledgements.
This work was supported by the Ministry of Education (Malaysia) through Fundamental Research Grant Scheme (FRGS/1/2020/STG06/UPM/02/1).

References

[1] K. Bhattacharyya, G.C. Layek, and G.S. Seth. Soret and Dufour effects on convective heat and mass transfer in stagnation-point flow towards a shrinking surface. *Physica Scripta*, vol. 89 (2014), no. 9, p. 095203.

[2] D. Pal and H. Mondal. Influence of soret and Dufour on MHD buoyancy-driven heat and mass transfer over a stretching sheet in porous media with temperature-dependent viscosity. *Nuclear Engineering and Design*, vol. 256 (2013), pp. 350–357.

[3] T. Hayat, A. Shafiq, and A. Alsaedi. Effect of joule heating and thermal radiation in flow of third grade fluid over radiative surface. *PLoS ONE*, vol. 9 (2014), no. 1, p. e83153.

[4] M. Ramzan, S. Inam, and S.A. Shehzad. Three dimensional boundary layer flow of a viscoelastic nanofluid with soret and Dufour effects. *Alexandria Engineering Journal*, vol. 55 (2016), no. 1, pp. 311–319.

[5] M.B. Ashraf, T. Hayat, A. Alsaedi, and S.A. Shehzad. Soret and Dufour effects on the mixed convection flow of an Oldroyd-B fluid with convective boundary conditions. *Results in Physics*, vol. 6 (2016), pp. 917–924.

[6] A. Farooq, R. Ali, and A.C. Benim. Soret and Dufour effects on three dimensional Oldroyd-B fluid. *Physica A: Statistical Mechanics and its Applications*, vol. 503 (2018), pp. 345–354.

[7] T. Hayat, F.M. Abbasi, S. Obaidat. Peristaltic motion with Soret and Dufour effects. *Magnetohydrodynamics*, vol. 47 (2011), no. 3, pp. 295–302; DOI: http://10.22364/mhd.47.3.8

[8] D. Pal, G. Mandal, and K. Vajravalu. Soret and Dufour effects on MHD convective–radiative heat and mass transfer of nanofluids over a vertical non-linear stretching/shrinking sheet. *Applied Mathematics and Computation*, vol. 287–288 (2016), pp. 184–200.

[9] I. Ullah, I. Khan, and S. Shafie. Soret and Dufour effects on unsteady mixed convection slip flow of Casson fluid over a nonlinearly stretching sheet with convective boundary condition. *Scientific Reports*, vol. 7 (2017), pp. 1113.

[10] D. Srinivasacharya and C. RamReddy. Soret and Dufour effects on mixed convection from an exponentially stretching surface. *International Journal of Nonlinear Science*, vol. 12 (2011), no. 1, pp. 60–68.

[11] P. Sreenivasulu and N.B. Reddy. Soret and Dufour effects on boundary layer flow past an exponential stretching sheet with thermal radiation and viscous dissipation. *Applied Mathematics*, vol. 51 (2012), pp. 10809–10816.

[12] T. Hayat, T. Muhammad, S.A. Shehzad, and A. Alsaedi. Soret and Dufour effects in three-dimensional flow over an exponentially stretching surface with porous medium, chemical reaction and heat source/sink. *International Journal of Numerical Methods for Heat and Fluid Flow*, vol. 25 (2015), no. 4, pp. 762–781.

[13] K. Sharada and B. Shankar. MHD mixed convection flow of a Casson fluid over an exponentially stretching surface with the effects of Soret, Dufour, thermal radiation and chemical reaction. *World Journal of Mechanics*, vol. 5 (2015), pp. 165–177.

[14] S.S.P.M. Isa, N.M. Arifin, and U. Farooq. Effect of Soret and Dufour numbers on double diffusive mixed convection boundary layer flow induced by a shrinking sheet. *Journal of Physics: Conference Series*, vol. 1298 (2019), p. 012024.

[15] C. Sravanthi. Homotopy analysis solution of MHD slip flow past an exponentially stretching inclined sheet with Soret-Dufour effects. *Journal of the Nigerian Mathematical Society*, vol. 35 (2016), no. 1, pp. 208–226.

[16] K.V.C. Sekhar and V. Manjula. MHD slip flow of Casson fluid over an exponentially stretching inclined permeable sheet with Soret–Dufour effects. *International Journal of Civil Engineering and Technology*, vol. 9 (2018), no. 3, pp. 400–417.

[17] H. Mondal, D. Pal, S. Chatterjee, and P. Sibanda. Thermophoresis and Soret-Dufour on MHD mixed convection mass transfer over an inclined plate with non-uniform heat source/sink and chemical reaction. *Ain Shams Engineering Journal*, vol. 9 (2018), no. 4, pp. 2111–2121.

[18] T. Hayat, Y. Saeed, S. Asad, and A. Alsaedi. Convective heat and mass transfer in flow by an inclined stretching cylinder. *Journal of Molecular Liquids*, vol. 220 (2016), pp. 573–580.

[19] N. Ahmed, S. Sengupta. Thermo-diffusion and diffusion-thermo effects on a three dimensional MHD mixed convection flow past an infinite vertical porous plate with thermal radiation. *Magnetohydrodynamics*, vol. 47 (2011), no. 1, pp. 41–60; DOI: http://doi.org/10.22364/mhd.47.1.5

[20] W. Jamshed and K.S. Nisar. Computational single-phase comparative study of a Williamson nanofluid in a parabolic trough solar collector via the Keller box method. *International Journal of Energy Research*, vol. 45 (2021), no. 7, pp. 10696–10718.

[21] W. Jamshed, E.K. Akgül, and K.S. Nisar. Keller box study for inclined magnetically driven Casson nanofluid over a stretching sheet: Single phase model. *Physica Scripta*, vol. 96 (2021), no. 6, p. 065201.

[22] W. Jamshed, S.U. Devi, and K.S. Nisar. Single phase based study of Ag-Cu/EO Williamson hybrid nanofluid flow over a stretching surface with shape factor. *Physica Scripta*, vol. 96 (2021), no. 6, p. 065202.

[23] W. Jamshed, K.S. Nisar, R.J.P. Gowda, R.N. Kumar and B.C. Prasannakumara. Radiative heat transfer of second grade nanofluid flow past a porous flat surface: A single-phase mathematical model. *Physica Scripta*, vol. 96 (2021), no. 6, p. 064006.

[24] T. Hayat, T. Nasir, M.I. Khan, and A. Alsaedi. Numerical investigation of MHD flow with Soret and Dufour effect. *Results in Physics*, vol. 8 (2018), pp. 1017–1022.

[25] N. Dzulkifli, N. Bachok, I. Pop, N.A. Yacob, N.M. Arifin and H. Rosali. Stability of partial slip, Soret and Dufour effects on unsteady boundary layer flow and heat transfer in copper-water nanofluid over a stretching/shrinking sheet. *Journal of Physics: Conference Series*, vol. 890 (2017), p. 012031.

[26] N. Dzulkifli, N. Bachok, I. Pop, N.A. Yacob, N.M. Arifin and H. Rosali. Soret and Dufour effects on unsteady boundary layer flow and heat transfer of nanofluid over a stretching/shrinking sheet: A stability analysis. *Journal of Chemical Engineering and Process Technology*, vol. 8 (2017), no. 3, pp. 1–10.

[27] N. Najib, N. Bachok, N.M. Arifin, and F.M. Ali. Stability analysis of stagnation-point flow in a nanofluid over a stretching/shrinking sheet with second-order slip, Soret and Dufour effects: A revised model. *Applied Sciences*, vol. 8 (2018), no. 4, p. 642.

[28] S. Parvin, S.S.P.M. Isa, N.M. Arifin, and F.M. Ali. The magnetohydrodynamics Casson fluid flow, heat and mass transfer due to the presence of assisting flow and buoyancy ratio parameters. *CFD Letters*, vol. 12 (2020), no. 8, pp. 64–75.

[29] S. Parvin, S.S.P.M. Isa, N.M. Arifin, and F.M. Ali. Dual numerical solutions on mixed convection Casson fluid flow due to the effect of the rate of extending and compressing sheet–stability analysis. *CFD Letters*, vol. 12 (2020), no. 8, pp. 76–84.

[30] T. Hayat, A. Shafiq, A. Alsaedi, and S. Asghar. Effect of inclined magnetic field in flow of third grade fluid with variable thermal conductivity. *AIP Advances*, vol. 5 (2015), no. 8, p. 087108.

[31] S.S.P.M. Isa, N.M. Arifin, R. Nazar, N. Bachok, F.M. Ali, and I. Pop. MHD mixed convection boundary layer flow of a Casson fluid bounded by permeable shrinking sheet with exponential variation. *Scientia Iranica*, vol. 24 (2017), no. 2, pp. 637–647.

[32] P.D. Weidman, D.G. Kubitschek, and A.M.J. Davis. The effect of transpiration on self-similar boundary layer flow over moving surfaces. *International Journal of Engineering Science*, vol. 44 (2006), pp. 730–737.

[33] S.D. Harris, D.B. Ingham, and I. Pop. Mixed convection boundary-layer flow near the stagnation point on a vertical surface in a porous medium: Brinkman model with slip. *Transport in Porous Media*, vol. 77 (2009), no. 2, pp. 267–285.

[34] E. Magyari and B. Keller. Heat and mass transfer in the boundary layers on an exponentially stretching continuous surface. *Journal of Physics D: Applied Physics*, vol. 32 (1999), no. 5, pp. 577–585.

Received 15.07.2021